A residue-based mode selection and sorting procedure for efficient poroelastic modeling in acoustic finite element applications

Romain Rumpler, Peter Göransson, Jean-François Deü

A residue-based mode selection and sorting procedure for efficient poroelastic modeling in acoustic finite element applications

Romain Rumpler[a] **and Peter Goransson**
The Marcus Wallenberg Laboratory for Sound and Vibration Research (MWL), Department of Aeronautical and Vehicle Engineering, KTH Royal Institute of Technology, School of Engineering Sciences, SE-10044 Stockholm, Sweden.

Jean-François Deü
Structural Mechanics and Coupled Systems Laboratory (LMSSC), Conservatoire National des Arts et Metiers (CNAM), Mechanics-case 2D6R10-2 Rue Conte 75003, Paris, France.

Analysis of three-dimensional sound propagation in porous elastic media with the Finite Element (FE) method is, in general, computationally costly. Although it is the most commonly used predictive tool in complex noise control applications, efficient FE solution strategies for large-size industrial problems are still lacking. In this work, an original procedure is proposed for the sorting and selection of the modes in the solution for the sound field in homogeneous porous domains. This procedure, validated on several 2D and 3D problems, enables to reduce the modal basis in the porous medium to its most physically significant components. It is shown that the size of the numerical problem can be reduced, together with matrix sparsity improvements, which lead to the reduction in computational time and enhancements in the efficacy of the acoustic response computation. The potential of this method for other industrial-based noise control problems is also discussed.

I. INTRODUCTION

Porous materials, as a passive solution for noise reduction in vehicles, have been widely investigated over the past two decades. Their modeling, in acoustic applications, has been particularly supported by the Biot-Allard theory of wave propagation in sound absorbing porous materials, tracing back to the early analyses by Biot for the modeling of a homogenized medium consisting of a porous elastic skeleton containing a viscous fluid,[1,2] later extended to include anisotropy as well as a refined description of viscoelastic and solid dissipations.[3] The refined theory has emerged as a reference to describe the complex physics involved.[4] Substantial efforts have been carried out to propose efficient predictive tools, a requirement to allow industrial applications to be performed at a reasonable cost, i.e., time and computational resources. Among these tools, the Finite Element (FE) method has been used extensively, due to its ability to accurately model a wide range of applications with complex geometries. When used for porous materials modeling, it however suffers from a high computational cost, both due to the costly formulations, involving four[5] to six[6] degrees of freedom (DOF) per node, and the need to refine the discretization with, e.g., increasing geometric complexity, or frequency range. Furthermore, modeling poroelastic materials requires particularly refined meshes, as shorter wavelengths need to be resolved as compared to more classic conservative acoustic applications. In addition, the generated system of linear equations is complex and frequency-dependent, implying an increased amount of resources needed to solve the problem, both in terms of computational time and memory allocation. In an attempt to improve the efficiency associated with FE modeling of sound absorbing porous materials, recent contributions have been made on the use of reduced order models, and particularly the use of a modal approach. In Ref. 7, generalized complex modes were used to reduce poroelastic domains, described with the mixed displacement-pressure formulation. The method was shown to be difficult to apply in an industrial context. The solid phase and fluid phase displacements formulation[6] was used in Refs. 8 and 9 to iteratively derive an appropriate porous modal basis, stating the estimated performance of the respective methods in terms of number of dofs and precision only. Recently, Dazel *et al.* used their 6-DOF-per-node formulation to propose resolution methods based on normal modes for the poroelastic equations.[10,11] However, the associated modal-based solutions proposed were either derived under the assumption of neglected shear in the porous material,[10] or demonstrated on unidimensional applications, thus not involving shear waves.[11] In a previous contribution, the authors introduced an original modal approach based on standard real-valued porous modes, using the solid and fluid phase displacements poroelastic formulation.[6] While the method proved to be efficient against the most widely used formulations, and able to capture porous responses involving shear waves, it was however shown that, for 3D applications, the approach involved relatively large modal bases, the

[a]Author to whom correspondence should be addressed. Electronic mail: rumpler@kth.se

participation of which was uneven in the response, thus resulting in an unnecessarily slow convergence rate.

In the present contribution, the authors present a substantial enhancement to this modal approach, for the reduction of porous domains, validated in the scope of poro-acoustic applications. It aims at proposing a remedy to the previously mentioned shortcoming of the method: An original mode selection, sorting, and truncation procedure is proposed, in order to extract the porous modes most significantly contributing to the physical content of the acoustic response. It results in a further reduced model thus improving the efficacy of the FE modeling of poro-acoustic problems. The first section recalls, in a condensed way, the general poro-acoustic problem used, as well as the main equations leading to the corresponding FE formulation for time-harmonic excitations. The next section briefly recalls the modal approach as proposed in Ref. 12, and introduces the original sorting and mode-selection procedure, based on the use of residual vectors, which is presented in detail. The third section of this work is dedicated to numerical applications. A small bi-dimensional poro-acoustic example is first presented, in order to illustrate the issues mentioned in Ref. 12, and the improvements offered by the proposed approach. These improvements are further illustrated on a more complex bi-dimensional application, before quantifying its potential and performance on the 3D example previously used in Ref. 12. Complementary plots for the results presented in this contribution can be found in Ref. 13. Perspectives to the proposed approach are given in conclusion to the paper.

II. FINITE ELEMENT FORMULATION FOR THE PORO-ACOUSTIC PROBLEM

A poro-acoustic problem is considered, whose description and notations are presented in Fig. 1. The formulation, as presented in this paper, is based on previous research published by the authors[12,14] for poro-elasto-acoustic and poro-acoustic applications. The acoustic fluid and the porous medium occupy the domains Ω_F and Ω_P, respectively. The compressible fluid is described using the pressure fluctuation (p) as primary variable (Sec. II A 1), while fluid and solid phases homogenized displacements ($\mathbf{u}_s$, $\mathbf{u}_f$) are retained as primary variables for the porous media (Sec. II A 2). The boundaries of the domain are separated into contours of (1) imposed Dirichlet boundary conditions denoted $\partial_1\Omega_F$ and $\partial_1\Omega_P$, (2) prescribed Neumann boundary conditions denoted $\partial_2\Omega_F$ and $\partial_2\Omega_P$, (3) coupling interface between acoustic fluid and porous media (Γ_{FP}).

In the following, a condensed summary of the main equations is given in order to establish the FE formulation, which is presented for a stationary harmonic response at angular frequency ω. For completeness, further details of the derivation can be found in Ref. 12.

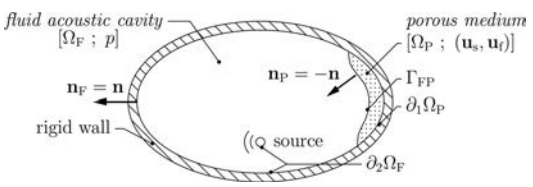

FIG. 1. Description and notations of the poro-acoustic interaction problem.

A. Dynamic equations and constitutive laws

1. Compressible fluid (p)

The internal fluid within cavities is supposed to be compressible, inviscid, and governed by the Helmholtz equation, assuming $\omega \neq 0$,

$$\Delta p + \frac{\omega^2}{c_0^2} p = 0 \quad \text{in } \Omega_F, \tag{1}$$

where c_0 is the constant speed of sound in the fluid, and p the pressure fluctuation scalar field.

2. Porous media Biot theory ($\mathbf{u}_s$, $\mathbf{u}_f$)

At angular frequency ω, the poroelastic medium satisfies the following elastodynamic linearized equations, in Ω_P, derived in the Biot-Allard theory[4] (see Table I for notations), taking into account inertia and viscous coupling effects between solid and fluid phases,

$$\operatorname{div}\boldsymbol{\sigma}_s + (\rho_a\omega^2 - i\omega\tilde{b}(\omega))(\mathbf{u}_s - \mathbf{u}_f) + (1-\phi)\rho_s\omega^2\mathbf{u}_s = \mathbf{0}, \tag{2a}$$

$$\operatorname{div}\boldsymbol{\sigma}_f + (\rho_a\omega^2 - i\omega\tilde{b}(\omega))(\mathbf{u}_f - \mathbf{u}_s) + \phi\rho_f\omega^2\mathbf{u}_f = \mathbf{0}, \tag{2b}$$

where $\mathbf{u}_s$ and $\mathbf{u}_f$ are, respectively, the solid phase and fluid phase averaged displacements in the sense of the Biot theory. $\tilde{b}(\omega)$ (henceforth denoted $\tilde{b}$, where the tilde refers to a complex-valued quantity) and ρ_a are, respectively, the complex frequency-dependent viscous drag and the inertia coupling parameter,[4] given by

$$\tilde{b} = \sigma\phi^2\left[1 + \frac{4i\omega\alpha_\infty^2\eta\rho_f}{\sigma^2\Lambda^2\phi^2}\right]^{1/2}, \quad \text{and} \quad \rho_a = \phi\rho_f(\alpha_\infty - 1).$$

$\boldsymbol{\sigma}_s$ and $\boldsymbol{\sigma}_f$ are the averaged stress tensors for the solid and fluid phases, respectively. In Ref. 12, it was shown that they

TABLE I. Material parameters; notations and properties.

	Notation and Description	Mat. 1	Mat. 2
ρ_s	Frame material density [kg m^{-3}]	30	
$(E_s;\ \nu)$	Frame elastic properties [kPa; ∅]	(845; 0.3)	(270; 0.3)
ρ_f	Ambient fluid density [kg m^{-3}]	1.21	
η	Ambient fluid viscosity [kN s m^{-2}]	1.84×10^{-5}	
P_0	Ambient fluid standard pressure [kPa]	101	
γ	Ambient fluid heat capacity ratio [∅]	1.4	
Pr	Ambient fluid Prandtl number [∅]	0.71	
ϕ	Porosity [∅]	0.96	0.98
α_∞	Tortuosity [∅]	1.7	1.7
σ	Static flow resistivity [kN s m^{-4}]	32	13.5
Λ	Viscous characteristic length [μm]	90	80
Λ'	Thermal characteristic length [μm]	165	160

satisfy the Lagrangian stress-strain relations developed by Biot, rewritten in the following form using Voigt notation

$$\boldsymbol{\sigma}_\mathrm{s} = [\mathbf{D}_\mathrm{s}^{(1)} + (\tilde{K}_\mathrm{f} - P_0)\,\mathbf{D}_\mathrm{s}^{(2)}]\,\boldsymbol{\varepsilon}(\mathbf{u}_\mathrm{s}) + [\mathbf{D}_\mathrm{sf}^{(1)} + (\tilde{K}_\mathrm{f} - P_0)\,\mathbf{D}_\mathrm{sf}^{(2)}]\,\boldsymbol{\varepsilon}(\mathbf{u}_\mathrm{f}), \tag{3a}$$

$$\boldsymbol{\sigma}_\mathrm{f} = [\mathbf{D}_\mathrm{sf}^{(1)} + (\tilde{K}_\mathrm{f} - P_0)\,\mathbf{D}_\mathrm{sf}^{(2)}]\,\boldsymbol{\varepsilon}(\mathbf{u}_\mathrm{s}) + [\mathbf{D}_\mathrm{f}^{(1)} + (\tilde{K}_\mathrm{f} - P_0)\,\mathbf{D}_\mathrm{f}^{(2)}]\,\boldsymbol{\varepsilon}(\mathbf{u}_\mathrm{f}), \tag{3b}$$

where $\boldsymbol{\varepsilon}(\mathbf{u}_\mathrm{s})$ and $\boldsymbol{\varepsilon}(\mathbf{u}_\mathrm{f})$ are the strain tensors associated with the averaged displacements vector fields $\mathbf{u}_\mathrm{s}$ and $\mathbf{u}_\mathrm{f}$, respectively. $\tilde{K}_\mathrm{f}(\omega)$ is the effective bulk modulus of the fluid phase (henceforth denoted $\tilde{K}_\mathrm{f}$); $\mathbf{D}_\mathrm{s}^{(1),(2)}$, $\mathbf{D}_\mathrm{f}^{(1),(2)}$, and $\mathbf{D}_\mathrm{sf}^{(1),(2)}$ are constant real-valued constitutive matrices detailed in Ref. 12.

B. Fluid-structure interaction problem

1. Poro-acoustic coupling and boundary conditions

At external boundary of the acoustic domain, rigid walls are considered, imposing a free pressure field ($\partial_1\Omega_\mathrm{F} = \emptyset$). The time-harmonic source term is given by

$$\mathbf{grad}\, p \cdot \mathbf{n} = \omega^2 \rho_\mathrm{F} u_\mathrm{Fb} \quad \text{on } \partial_2\Omega_\mathrm{F}, \tag{4}$$

where u_Fb is non-zero at the acoustic source location only (see $\partial_2\Omega_\mathrm{F}$ in Fig. 1).

Coupling at interface Γ_FP is given by normal stress and normal displacement continuity conditions between the acoustic fluid and both fluid and solid phases of the porous medium:

$$\boldsymbol{\sigma}_\mathrm{s}\,\mathbf{n} + (1-\phi)\,p\,\mathbf{n} = \mathbf{0} \quad \text{on} \quad \Gamma_\mathrm{FP}, \tag{5a}$$

$$\boldsymbol{\sigma}_\mathrm{f}\,\mathbf{n} + \phi\,p\,\mathbf{n} = \mathbf{0} \quad \text{on} \quad \Gamma_\mathrm{FP}, \tag{5b}$$

$$\mathbf{u}_\mathrm{F}\cdot\mathbf{n} - (1-\phi)\mathbf{u}_\mathrm{s}\cdot\mathbf{n} - \phi\mathbf{u}_\mathrm{f}\cdot\mathbf{n} = 0 \quad \text{on} \quad \Gamma_\mathrm{FP}, \tag{6}$$

where ϕ is the porosity of the porous material, i.e., the volume fraction of fluid.

No external force is applied to the outer boundary of the porous medium except along interface Γ_FP. Therefore, $\partial_2\Omega_\mathrm{P} = \emptyset$ in the considered problems. Finally, at the external boundary $\partial_1\Omega_\mathrm{P}$, two types of boundary conditions may be prescribed, as detailed in Ref. 12, the porous material being considered either as sliding or bonded to a rigid wall.

2. Finite element discretized problem

The test-function method is used to derive the variational formulation of the coupled problem. Details can be found in Refs. 12 and 14. Thus, using the Helmholtz equation (1), the poroelastic dynamic Eqs. (2a) and (2b), the constitutive expressions (3a) and (3b), as well as the excitation and coupling conditions (4), (6), (5a) and (5b), the following discretized system of equations arises:

$$\left(\begin{bmatrix} \mathbf{K}_\mathrm{F} & \mathbf{0} & \mathbf{0} \\ -(1-\phi)\mathbf{A}_\mathrm{Fs}^T & \mathbf{K}_\mathrm{ss}^{(1)} & \mathbf{K}_\mathrm{sf}^{(1)} \\ -\phi\mathbf{A}_\mathrm{Ff}^T & \mathbf{K}_\mathrm{sf}^{(1)T} & \mathbf{K}_\mathrm{ff}^{(1)} \end{bmatrix} + (\tilde{K}_\mathrm{f} - P_0) \begin{bmatrix} \mathbf{0} & \mathbf{0} & \mathbf{0} \\ \mathbf{0} & \mathbf{K}_\mathrm{ss}^{(2)} & \mathbf{K}_\mathrm{sf}^{(2)} \\ \mathbf{0} & \mathbf{K}_\mathrm{sf}^{(2)T} & \mathbf{K}_\mathrm{ff}^{(2)} \end{bmatrix} + \mathrm{i}\omega\tilde{b} \begin{bmatrix} \mathbf{0} & \mathbf{0} & \mathbf{0} \\ \mathbf{0} & \mathbf{C}_\mathrm{ss} & \mathbf{C}_\mathrm{sf} \\ \mathbf{0} & \mathbf{C}_\mathrm{sf}^T & \mathbf{C}_\mathrm{ff} \end{bmatrix} - \omega^2 \begin{bmatrix} \mathbf{M}_\mathrm{F} & (1-\phi)\mathbf{A}_\mathrm{Fs} & \phi\mathbf{A}_\mathrm{Ff} \\ \mathbf{0} & \mathbf{M}_\mathrm{ss} & \mathbf{M}_\mathrm{sf} \\ \mathbf{0} & \mathbf{M}_\mathrm{sf}^T & \mathbf{M}_\mathrm{ff} \end{bmatrix} \right) \begin{bmatrix} \mathbf{P} \\ \mathbf{U}_\mathrm{s} \\ \mathbf{U}_\mathrm{f} \end{bmatrix} = \begin{bmatrix} \omega^2\mathbf{U}_\mathrm{Fb} \\ \mathbf{0} \\ \mathbf{0} \end{bmatrix}. \tag{7}$$

This non-symmetric formulation can be symmetrized by dividing the acoustic equation by ω^2 ($\omega \neq 0$).

III. MODAL REDUCTION OF THE POROELASTIC MEDIUM

A. Presentation of the typical poro-acoustic test case

The proposed modal-based reduction is applied to the porous domain of a poro-acoustic problem, where the acoustic domain is kept unreduced. Within the acoustic domain, the degrees of freedom (dofs) are separated into internal ones (subscript $\bar{I}$), and those at interface with the porous medium (subscript I). These notations, consistent with previous works by the authors,[12,14] allow for an extension of the method to problems with multiple interfaces, though considered out of the scope of the present contribution. In addition, the solid and fluid phase dofs (subscripts s and f, respectively) are further denoted by a common set of porous dofs (subscript P), such that the matrix system of equations (7) may be rewritten as

$$\begin{bmatrix} \mathbf{K}_{\bar{I}\bar{I}} - \omega^2\mathbf{M}_{\bar{I}\bar{I}} & \mathbf{K}_{\bar{I}I} - \omega^2\mathbf{M}_{\bar{I}I} & \mathbf{0} \\ \mathbf{K}_{I\bar{I}} - \omega^2\mathbf{M}_{I\bar{I}} & \mathbf{K}_{II} - \omega^2\mathbf{M}_{II} & -\omega^2\mathbf{A}_{I\mathrm{P}} \\ \mathbf{0} & -\mathbf{A}_{I\mathrm{P}}^T & \mathbf{K}_\mathrm{P}^{(1)} + (\tilde{K}_\mathrm{f} - P_0)\,\mathbf{K}_\mathrm{P}^{(2)} + \mathrm{i}\omega\tilde{b}\mathbf{C}_\mathrm{P} - \omega^2\mathbf{M}_\mathrm{P} \end{bmatrix} \begin{bmatrix} \mathbf{P}_{\bar{I}} \\ \mathbf{P}_I \\ \mathbf{U}_\mathrm{P} \end{bmatrix} = \begin{bmatrix} \omega^2\mathbf{U}_{\bar{I}\mathrm{b}} \\ \mathbf{0} \\ \mathbf{0} \end{bmatrix}, \tag{8}$$

which can be symmetrized by dividing the acoustic equations by ω^2 ($\omega \neq 0$), and where $\mathbf{A}_{I\mathrm{P}}$ is the coupling matrix between the interface acoustic dofs (subscript I) and the porous dofs (subscript P), given by $\mathbf{A}_{I\mathrm{P}} = [\,(1-\phi)\mathbf{A}_{I\mathrm{s}} \quad \phi\mathbf{A}_{I\mathrm{f}}\,]$.

B. Modal-based reduction of the homogeneous porous domain

From the proposed expression of the porous media FE problem, real-valued normal modes can be computed associated with the coupled poroelastic eigenvalue problem[12]

$$(\mathbf{K}_{\mathrm{P}}^{(1)} - \omega^2 \mathbf{M}_{\mathrm{P}})\phi = \mathbf{0}. \tag{9}$$

It is supposed that the Dirichlet boundary conditions imposed result in a nonsingular $\mathbf{K}_{\mathrm{P}}^{(1)}$ matrix, therefore removing zero-frequency modes. A modal reduction basis $\mathbf{\Phi}_{\mathrm{P}m}$ is built, selecting the m lowest-frequency modes. They are normalized with respect to the porous mass matrix $\mathbf{M}_{\mathrm{P}}$ so that $\mathbf{\Phi}_{\mathrm{P}m}^T \mathbf{M}_{\mathrm{P}} \mathbf{\Phi}_{\mathrm{P}m} = \mathbf{I}_m$, and $\mathbf{\Phi}_{\mathrm{P}m}^T \mathbf{K}_{\mathrm{P}}^{(1)} \mathbf{\Phi}_{\mathrm{P}m} = \mathbf{\Omega}_m$, where $\mathbf{I}_m$ is a unit matrix of dimension m, and $\mathbf{\Omega}_m$ a diagonal matrix with the m lowest eigenvalues of Eq. (9) on its diagonal. It was shown in Ref. 12 that such a truncated modal basis exhibits close to orthogonality properties with respect to the global matrices $\mathbf{K}_{\mathrm{P}}^{(2)}$ and $\mathbf{C}_{\mathrm{P}}$, implying sparsely populated associated matrices $\boldsymbol{\kappa}_m$ and $\boldsymbol{\zeta}_m$, defined as $\mathbf{\Phi}_{\mathrm{P}m}^T \mathbf{C}_{\mathrm{P}} \mathbf{\Phi}_{\mathrm{P}m} = \boldsymbol{\zeta}_m$, and $\mathbf{\Phi}_{\mathrm{P}m}^T \mathbf{K}_{\mathrm{P}}^{(2)} \mathbf{\Phi}_{\mathrm{P}m} = \boldsymbol{\kappa}_m$, respectively.

The transformation, leading to a reduced version of system (8), keeping acoustic dofs uncondensed, is completed by a set of linearly independent attachment functions, linking the interface acoustic dofs to the porous dofs. They are computed as the $\mathbf{K}_{\mathrm{P}}^{(1)}$–static responses of the porous medium to unit pressure successively imposed to each interface acoustic dof, i.e., $\mathbf{\Psi}_{\mathrm{P}I} = \mathbf{K}_{\mathrm{P}}^{(1)^{-1}} \mathbf{A}_{I\mathrm{P}}{}^T$.

The corresponding change of basis, leaving acoustic dofs uncondensed, is then

$$\begin{bmatrix} \hat{\mathbf{P}}_{\bar{I}} \\ \hat{\mathbf{P}}_I \\ \hat{\mathrm{U}}_{\mathrm{P}} \end{bmatrix} = \begin{bmatrix} \mathbf{I}_{\bar{I}} & 0 & 0 \\ 0 & \mathbf{I}_I & 0 \\ 0 & \mathbf{\Psi}_{\mathrm{P}I} & \mathbf{\Phi}_{\mathrm{P}m} \end{bmatrix} \begin{bmatrix} \hat{\mathbf{P}}_{\bar{I}} \\ \hat{\mathbf{P}}_I \\ \hat{\alpha}_m \end{bmatrix}, \tag{10}$$

where $\widehat{(.)}$ denotes an approximation of the original solution, and $\hat{\boldsymbol{\alpha}}_m$ is the vector of modal coordinates. When applied to a symmetrized form of Eq. (8), the transformation leads to the following reduced set of equations,

$$\begin{bmatrix} \frac{1}{\omega^2}\mathbf{K}_{\bar{I}\bar{I}} - \mathbf{M}_{\bar{I}\bar{I}} & \frac{1}{\omega^2}\mathbf{K}_{\bar{I}I} - \mathbf{M}_{\bar{I}I} & \mathbf{0} \\ \frac{1}{\omega^2}\mathbf{K}_{I\bar{I}} - \mathbf{M}_{I\bar{I}} & \frac{1}{\omega^2}\mathbf{K}_{II} - \mathbf{M}_{II} - \mathbf{K}_{\mathrm{P}_{II}}^{(1)} + (\tilde{K}_{\mathrm{f}} - P_0)\,\mathbf{K}_{\mathrm{P}_{II}}^{(2)} + \mathrm{i}\omega\tilde{b}\mathbf{C}_{\mathrm{P}_{II}} - \omega^2\mathbf{M}_{\mathrm{P}_{II}} & (\tilde{K}_{\mathrm{f}} - P_0)\,\mathbf{K}_{\mathrm{P}_{Im}}^{(2)} + \mathrm{i}\omega\tilde{b}\mathbf{C}_{\mathrm{P}_{Im}} - \omega^2\mathbf{M}_{\mathrm{P}_{Im}} \\ \mathbf{0} & (\tilde{K}_{\mathrm{f}} - P_0)\,\mathbf{K}_{\mathrm{P}_{mI}}^{(2)} + \mathrm{i}\omega\tilde{b}\mathbf{C}_{\mathrm{P}_{mI}} - \omega^2\mathbf{M}_{\mathrm{P}_{mI}} & \mathbf{\Omega}_m + (\tilde{K}_{\mathrm{f}} - P_0)\,\boldsymbol{\kappa}_m + \mathrm{i}\omega\tilde{b}\tilde{\boldsymbol{\zeta}}_m - \omega^2\mathbf{I}_m \end{bmatrix} \begin{bmatrix} \hat{\mathbf{P}}_{\bar{I}} \\ \hat{\mathbf{P}}_I \\ \hat{\boldsymbol{\alpha}}_m \end{bmatrix} = \begin{bmatrix} \mathbf{U}_{\mathrm{Fb}} \\ \mathbf{0} \\ \mathbf{0} \end{bmatrix}, \tag{11}$$

where for porous matrices indexed by subscript P, i.e., $\mathbf{B}_{\mathrm{P}} \in \{\mathbf{K}_{\mathrm{P}}^{(1)}, \mathbf{K}_{\mathrm{P}}^{(2)}, \mathbf{C}_{\mathrm{P}}, \mathbf{M}_{\mathrm{P}}\}$, one has $\mathbf{B}_{\mathrm{P}_{II}} = \mathbf{\Psi}_{\mathrm{P}I}^T \mathbf{B}_{\mathrm{P}} \mathbf{\Psi}_{\mathrm{P}I}$, and $\mathbf{B}_{\mathrm{P}_{Im}} = \mathbf{\Psi}_{\mathrm{P}I}^T \mathbf{B}_{\mathrm{P}} \mathbf{\Phi}_{\mathrm{P}m} = \mathbf{B}_{\mathrm{P}_{mI}}^T$. This reduced model for homogeneous poroelastic materials, proposed in Ref. 12, was shown to be computationally efficient, especially considering the fact that the modal coordinates associated with the linearly independent poroelastic equations can be further condensed. However, the two following issues were observed: (1) a large amount of modes are required when following the rule of thumb of 1.5 to 2.5 times the highest frequency of interest for truncation, even though most seem to have little significant contribution, and (2) the convergence is not smooth with respect to the frequency when modes are added into the basis, which suggests that the modes are not satisfyingly ordered if sorted according to their eigenfrequencies. In the following, after introduction of an *a posteriori* error estimator, a selection and sorting procedure is proposed in order to overcome the obstacles presented by these two aspects.

C. *A posteriori* error estimation

For a given approximation of the solution using a reduced model, the error with respect to the unreduced solution can be estimated from the residue associated with the time-harmonic response. Thus, at a given angular frequency ω, the approximate solution, following the resolution of a set of equations such as Eq. (11), is given by the transformation of Eq. (10). From this approximate solution, using the last set of equations in Eq. (8), a residual force vector for the porous domain may be computed as

$$\begin{aligned} \mathbf{R}_{\mathrm{F_P}}(\omega) = \mathbf{A}_{I\mathrm{P}}^T \hat{\mathbf{P}}_I - (\,&\mathbf{K}_{\mathrm{P}}^{(1)} + (\tilde{K}_{\mathrm{f}}(\omega) - P_0)\,\mathbf{K}_{\mathrm{P}}^{(2)} \\ &+ \mathrm{i}\omega\tilde{b}(\omega)\mathbf{C}_{\mathrm{P}} - \omega^2\mathbf{M}_{\mathrm{P}})\hat{\mathrm{U}}_{\mathrm{P}}. \end{aligned} \tag{12}$$

From this, a $\mathbf{K}_{\mathrm{P}}^{(1)}$-residual displacement vector can be established, $\mathbf{R}_{\mathrm{U_P}}(\omega) = \mathbf{K}_{\mathrm{P}}^{(1)-1} \mathbf{R}_{\mathrm{F_P}}(\omega)$. It may then be used to construct an error estimator, in analogy with the strain energy error estimator used in structural dynamics,[15] computed at selected frequencies as

$$\varepsilon(\omega) = \frac{\mathbf{R}_{\mathrm{U_P}}^T(\omega)\mathbf{K}_{\mathrm{P}}^{(1)}\mathbf{R}_{\mathrm{U_P}}(\omega)}{\hat{\mathrm{U}}_{\mathrm{P}}^T\mathbf{K}_{\mathrm{P}}^{(1)}\hat{\mathrm{U}}_{\mathrm{P}}} = \frac{\mathbf{R}_{\mathrm{U_P}}^T(\omega)\mathbf{R}_{\mathrm{F_P}}(\omega)}{\hat{\mathrm{U}}_{\mathrm{P}}^T\mathbf{K}_{\mathrm{P}}^{(1)}\hat{\mathrm{U}}_{\mathrm{P}}}. \tag{13}$$

In the examples considered in this work, where the mean quadratic pressure in the acoustic domains is used as a response output, an estimated error lower than 0.1 has

proved to be a conservative limit achieving satisfying level approximations for the frequency responses.

D. Sorting and filtering procedure of porous modal contributions

Considering the localized and complex phenomena within the poroelastic layer, making it highly dependent on the excitation itself, the modes computed using a standard eigenvalue solver clearly do not all have a relevant contribution to the response. Here, a selection based on the use of residual forces is therefore proposed in order to generate a more specific modal basis.

1. Modal contribution criterion using a residual force

One major advantage with the residual forces is that they provide a very useful insight into the quality of the reduced model, as they are directly linked to the approximation made.[15] Therefore, in the context of modal reduction, they have been used for different purposes. Among the main possibilities, residual responses may be added, once orthogonalized, in reduction bases that are built iteratively;[16] they may also be used to take into account additional terms not included in the eigenvalue problem,[17,18] or modified parameters in an optimization procedure.[19] In fact, the residue provides a natural way to correct the reduction basis as it includes missing components.[16]

In the present approach, where the aim is to determine a suitable basis for a given frequency range, the residual force is used to estimate the modal contribution of the modes. By doing so, only the main components, properly describing the specific problem at hand, are kept in a further reduced basis. The residual force is computed, at a given angular frequency ω_0, using the solution vector of a reduced model including only the very low frequency modes, e.g., the first mode, following Eq. (11). Thus, a poor approximate solution, at ω_0, is obtained after inverse transformation,

$$\begin{bmatrix} \hat{\mathbf{P}}_{\bar{I}} \\ \hat{\mathbf{P}}_{I} \\ \hat{\mathbf{U}}_{\mathrm{P}} \end{bmatrix}_{\omega_0} = \begin{bmatrix} \mathbf{I}_{\bar{I}} & \mathbf{0} & \mathbf{0} \\ \mathbf{0} & \mathbf{I}_{I} & \mathbf{0} \\ \mathbf{0} & \mathbf{\Psi}_{\mathrm{P}I} & \mathbf{\Phi}_{\mathrm{P_{LF}}} \end{bmatrix} \begin{bmatrix} \hat{\mathbf{P}}_{\bar{I}} \\ \hat{\mathbf{P}}_{I} \\ \hat{\boldsymbol{\alpha}}_{\mathrm{LF}} \end{bmatrix}_{\omega_0}, \tag{14}$$

where $\mathbf{\Phi}_{\mathrm{P_{LF}}}$ consists of the lowest-frequency mode computed by solving eigenvalue problem (9), and $\hat{\boldsymbol{\alpha}}_{\mathrm{LF}}$ is the corresponding modal coordinate. Note that $\mathbf{\Phi}_{\mathrm{P_{LF}}}$ may include the first few modes with an advantage yet to be identified, but will be limited to the first mode in this manuscript. A residual force vector for the porous domain, $\mathbf{R}_{\mathrm{F_P}}(\omega_0)$, may then be computed following Eq. (12), at angular frequency ω_0, based on the approximate solution vector of Eq. (14). The subsequent $\mathbf{K}_{\mathrm{P}}^{(1)}$-residual displacement vector is then given by $\mathbf{R}_{\mathrm{U_P}}(\omega_0) = \mathbf{K}_{\mathrm{P}}^{(1)-1}\mathbf{R}_{\mathrm{F_P}}(\omega_0)$. The following step consists in comparing each mode shape to the content of this residue. An indicator such as the Modal Assurance Criterion (MAC) is an option that could be used for comparison between a residual displacement vector and the mode shapes, but does not carry significant physical meaning and is likely to bring inconclusive results. A concept such as the modal participation factors may bring a more significant answer to the present request. Thus, the participation factor of the ith mode shape $\mathbf{\Phi}_{\mathrm{P}i}$ to the real part of the $\mathbf{K}_{\mathrm{P}}^{(1)}$-residual displacement vector corresponding to the residual force $\mathbf{R}_{\mathrm{F}_j}$ [e.g., $\mathbf{R}_{\mathrm{F_P}}(\omega_0)$ associated with $\mathbf{\Phi}_{\mathrm{P_{LF}}}$ of Eq. (14)], is defined as

$$\mu_{ij} = \frac{|\mathbf{\Phi}_{\mathrm{P}i}^T \mathbf{M}_{\mathrm{P}} \mathbf{K}_{\mathrm{P}}^{(1)-1} \Re(\mathbf{R}_{\mathrm{F}_j})|}{||\Re(\mathbf{R}_{\mathrm{F}_j})||}. \tag{15}$$

For practical implementation purposes, it may be rewritten without the need to calculate the residual displacement vector. Using the eigenvalue problem Eq. (9), Eq. (15) becomes

$$\mu_{ij} = \frac{|\mathbf{\Phi}_{\mathrm{P}i} \cdot \Re(\mathbf{R}_{\mathrm{F}_j})|}{\omega_i{}^2 ||\Re(\mathbf{R}_{\mathrm{F}_j})||}, \tag{16}$$

where $\omega_i{}^2$ is the eigenvalue corresponding to the eigenvector $\mathbf{\Phi}_{\mathrm{P}i}$. An analogous definition can be given with respect to the imaginary part of $\mathbf{R}_{\mathrm{F}_j}$. The procedure thereafter described can also be applied to such an imaginary part participation factor but has shown no additional interest in the considered validation cases. It is recalled here that the eigenvector expression $\mathbf{\Phi}_{\mathrm{P}i}$ refers to a mass-normalized mode. This first approach enables a proper sorting of the mode shapes according to their modal participation to the residual vector. Furthermore, being independent of the residual force norm, the participation factors defined as such can be used to compare the relative contributions of a mode shape to a set of several residual force vectors computed at different frequencies. In the following, it is supposed that for a given residual force $\mathbf{R}_{\mathrm{F}_j}$, a set of N modes are ordered by decreasing modal participation such that $\mu_{1j} > \cdots > \mu_{ij} > \cdots > \mu_{\mathrm{N}j}$. In order to establish a truncation criterion based on these participation factors, they are normalized with respect to the smallest contribution, for a given residual force,

$$\forall\, i \in [1..\mathrm{N}]\ \bar{\mu}_{ij} = \frac{\mu_{ij}}{\mu_{\mathrm{N}j}} \geqslant 1. \tag{17}$$

In practice, these factors can differ from one another by several orders of magnitude, suggesting that a logarithmic scale would be more appropriate for their representation than a linear scale, as shown in Fig. 2. The logarithmic representation allows for a straightforward identification of the significant contributions, either by their contribution level, or by the change of the tangent slope, as may be observed in Fig. 2. Therefore, several selection criteria may be proposed, e.g., based on a threshold value, a gradient-based limit, or a ratio of contribution. After testing, the latter approach is presented in this work. Thus, a selection of the n most significant modes in the truncated modal basis is made using the following criterion, based on a ratio of the cumulated logarithmic contributions,

$$\chi_{\mathrm{n}j} = \frac{\sum_{i=1}^{\mathrm{n}} \log(\bar{\mu}_{ij})}{\sum_{i=1}^{\mathrm{N}} \log(\bar{\mu}_{ij})} \leqslant \chi_{\max}, \tag{18}$$

where $\chi_{\max}$ is an empirical limit, in the interval]0, 1], typically found to be conservatively suitable when set to 0.4 in the presented applications.

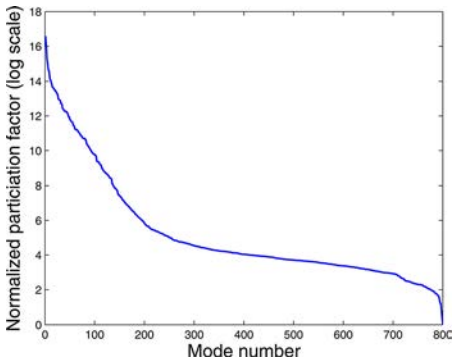

FIG. 2. (Color online) Example of normalized modal participation factors, logarithmic scale.

2. Procedure and practical implementation

The mode sorting indicator presented in Eq. (16), together with the selection criterion Eq. (18), are used for filtering mode shapes computed with the standard eigenvalue problem. The quasi-orthogonality property of the modes computed allows for them to be independently tested for their participation to the response content. For a small-sized problem involving the combination of a narrow frequency band and a low spectral density, one residual vector may be sufficient to select the proper modes. However, for applications with a broader frequency content, a selection based on several residual vectors distributed in the frequency range of interest is needed. Insofar as the numerical experiments conducted by the authors have shown, a rule of thumb of at least one residual vector per 400 porous modes, in 3D (ca. one per 250 to 300 porous modes in 2D), has proved to be sufficient when evenly distributing these vectors in the frequency range of interest. Two approaches may be considered, for a mode selection procedure based on a set of residual vectors, (1) the modes are ordered after a weighted average of their participation to the different residual vectors, or (2) the modes are successively selected according to their participation to the residual vectors ordered in increasing frequency. The first possibility imposes a weighting to be assigned to each residual vector, particularly in the aim of ordering the modes in the modal basis according to their influence in the frequency range. The second approach offers a natural weighting of the residual vectors, provided each of them is best suited for a frequency band centered on its frequency of computation. The latter method is chosen, selecting a set of modes with respect to the first residual vector, then completed by modes successively selected among the remaining ones, using the additional residual vectors. The corresponding procedure is detailed in Algorithm 1, outlined below.

IV. APPLICATIONS AND RESULTS

A. Illustration of the modal reduction limitations: A small bi-dimensional application

1. Presentation and reference solution

The simplified bi-dimensional model, used to illustrate the limitations of the direct modal approach, is presented in Fig. 3. It consists of an acoustic domain bounded by rigid walls, and treated with a porous layer on one wall (material 1^{20} in Table I), having sliding boundary conditions on the side walls and sticking to the back wall. The mesh, consisting of 7×5 linear elements both in the acoustic and porous domains, is suitable for an analysis up to 1500 Hz.

Algorithm 1: Procedure for selection of significant modes

1. Compute the truncated modal basis (eigenvalue problem)
2. Decompose $\mathbf{K}_{\mathrm{P}}^{(1)}$
3. Retain $\mathrm{N_{LF}}$ low frequency modes for residual vectors computation (typically $\mathrm{N_{LF}} = 1$)
4. Choose a set of ω_j for N_j residual vectors
5. Compute the corresponding $\mathbf{R}_{\mathrm{F}_j}$
6. Include the $\mathrm{N_{LF}}$ low frequency modes in the new basis
7. **for** $j = 1$ **to** N_j **do**
8. Compute μ_{ij} contributions for the modes not selected
9. Sort modes in descending μ_{ij} contribution
10. Compute the cumulated contributions $\chi_{\mathrm{n}j}$
11. Select modes for which $\chi_{\mathrm{n}j} \leqslant \chi_{\max}$
12. Add the sorted selected modes to the new basis
13. **end for**

The reference solution, with and without addition of the porous layer, is given in Fig. 4, using the mean quadratic pressure in the acoustic domain as a response quantity. For the solution without the porous layer, the porous domain is replaced by an acoustic domain in order to keep the dimensions of the cavity unchanged.

Such a small problem, both in terms of dimensions and frequency content, provides an insight into the convergence issues of the modal reduction, keeping the number of necessary modes reasonable.

2. Modal reduction and convergence enhancements

In a first step, the modal-based reduction as proposed in Ref. 12 is applied. In an attempt to keep the basis as small as possible, a satisfying convergence is achieved after a truncation of the modal basis to its 26 first contributions, i.e., up to 1343 Hz, which is more restrictive than the rule of thumb truncation criterion set to 1.5–2.5 times the highest frequency of interest. The corresponding coupled porous mode shapes are presented in Fig. 5.

From observation of these mode shapes, it is evident that they will exhibit uneven contributions to the actual response, hence the need for a filtering of the modal basis. For instance, some coupled mode shapes, in the low frequency range, show localized behavior more likely to be observed at higher frequencies or for specific excitations, e.g., modes 6, 8, 10, 11, 14, 19, 20, 22, 23 when compared to

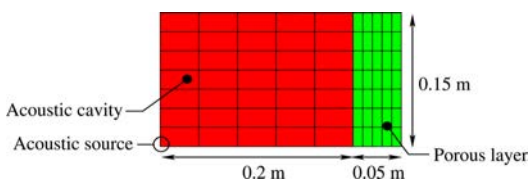

FIG. 3. (Color online) Mesh and dimensions of small 2D application.

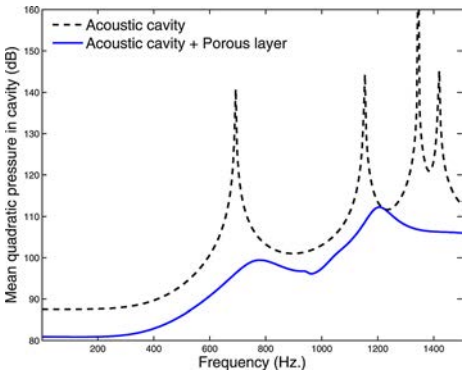

FIG. 4. (Color online) Mean quadratic pressure in the acoustic domain.

modes such as 1, 2, 12, 15, 21. The convergence to the reference solution is presented in Figs. 7(a)–7(c).

It is thus found that (1) the convergence is relatively slow with respect to the addition of modes in the basis, and (2) the eigenfrequency-based sorting of the modes does not necessarily match their frequency range of influence. For instance, including the first 15 modes in the basis implies precision improvements in the 500 and 900 Hz regions although the response is not yet converged below 400 Hz.

The modal basis refinement procedure proposed in this paper is therefore applied to the 26-mode basis in order to evaluate its potential. In this small application, one residual vector is retained for the mode selection procedure. This residual vector is computed with the lowest frequency mode included in the modal basis, and for an arbitrarily chosen low frequency of 375 Hz. The upper bound for cumulated contributions, $\chi_{\max}$, is set to 0.4. The thus selected significant modal contributions are the n modes satisfying $\chi_{nj} \leqslant 0.4$.

The mode selection following the sorting procedure is presented in Table II. The modal contribution associated with the first mode, which is included in the modal basis for computation of the residual vector, is given as an indication. It emphasizes the expected orthogonality between the mode shape and the residual vector computed with this mode included in the modal basis. In addition, it further confirms the established link, on which the selection procedure is based, between the residual vectors and the content of the modal basis. The first 8 selected and sorted mode shapes extracted from the complete modal basis (see Fig. 5) are presented in Fig. 6.

The convergence of the solution using a further reduced modal basis is presented in Figs. 7(d)–7(f). The precision achieved is already satisfactory when only the first 8 selected modes are included in the modal basis, which means that an upper bound of 0.38 for $\chi_{\max}$ was sufficient in this case. Finally, when compared to the convergence of the solution with unsorted modes in Figs. 7(a)–7(c), the proposed reordering strategy exhibits a significantly smoother convergence with respect to the frequency. For instance, using only the first four sorted modes results in a converged solution for more than the first half of the frequency range of interest. While only snapshots of the convergence are presented, a monotonic convergence was observed by adding each selected mode successively into the basis.

The computational time improvement and sparsity performance are not addressed in the 2D case. However, it can be underlined that the unreduced porous domain consists of 144 dofs, which are reduced to at best 26 dofs using a rule of thumb truncation of the complete modal basis. Use of the proposed selection procedure produces a further reduced poroelastic domain of at best 8 dofs, that is 5.5% of the original problem size, or 18 times smaller.

B. Bi-dimensional validation case

1. Presentation and reference solution

The application presented in the previous section is deliberately chosen small, both in terms of size and frequency content, in order to allow a detailed check of the mode filtering and sorting process, and thus to estimate the potential performance of the proposed criteria. However, due to its size, the problem tested is still rather close to a 1D problem, which is underlined by the selection of 1D mode shapes among the first modes selected. In this section, the established selection criterion is further tested on a larger 2D application, involving both

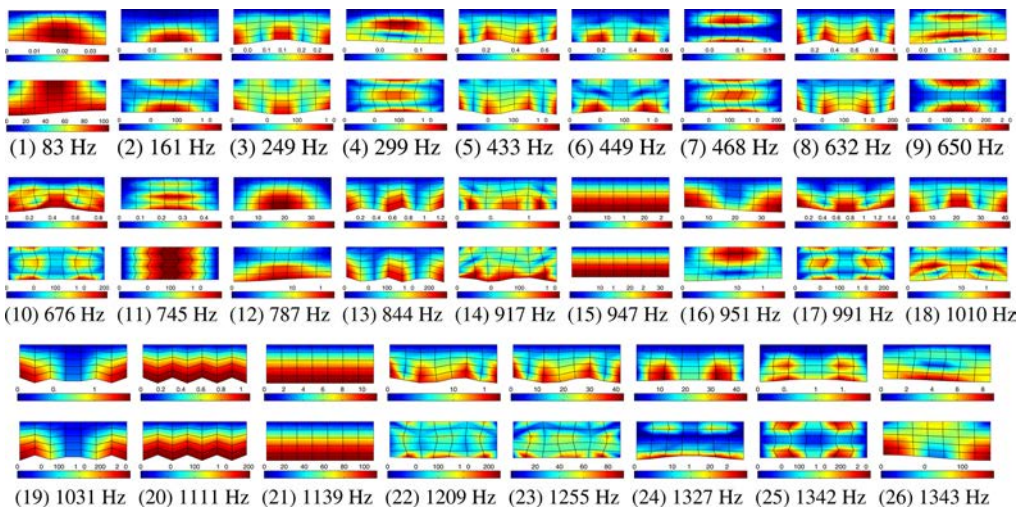

FIG. 5. (Color online) Two-dimensional porous mode shapes of modes 1–26: (top) solid and (bottom) fluid phases. Deformed mesh and magnitude of displacement ($\mathbf{M}_P$-normalized modes).

TABLE II. Significant modal contributions selection.

Mode	Eigenfrequency (Hz)	μ_{ij}	χ_{nj}
1	83	(0)	(1)
2	161	12.9	0.06
21	1139	12.0	0.12
15	947	11.9	0.17
4	299	11.1	0.23
12	787	10.4	0.28
26	1343	10.3	0.32
16	951	9.8	0.37
7	468	9.2	0.4

a broader frequency content and a proper 2D geometry. Its geometry, dimensions and mesh are presented in Fig. 8. The mesh, consisting of 40×13 linear elements in the acoustic domain and 40×12 linear elements in the porous domain (material 1^{20} in Table I), is well suited for an analysis up to 2000 Hz. In order to induce more shear waves into the layer, which should result in more modes to be selected in order to approximate the solution, all external porous boundaries are fixed, thus involving a problem with 574 acoustic dofs and 1935 poroelastic dofs. The acoustic domain is excited via a time-harmonic excitation at a corner of the acoustic cavity, opposite the porous layer. The reference solution, with and without the porous layer, is given in Fig. 9, using the mean quadratic pressure in the acoustic domain as an output (the porous domain is again replaced by acoustic elements in the conservative case).

2. Modal reduction and enhancements

The reduction is first made using the complete set of modes computed from the eigenvalue problem (9), with a rule of thumb truncation of twice the highest frequency of interest, i.e., for eigenfrequencies up to 4000 Hz. This involves 348 modes included in the basis. The convergence of the reduced solution is presented in Figs. 10(a)–10(c) for a modal basis truncated at significant steps including 91, 131, and 315 modes, for which convergence is reached. The previously observed convergence difficulties are exhibited, i.e., slow convergence and uneven contributions of the modes included in the basis.

The mode sorting and selection method is applied following the procedure in Algorithm 1. Considering the increased frequency content of the problem compared to the previous section, with more than 300 two-dimensional porous modes, two residual force vectors are used. They are computed with the lowest eigenfrequency mode included in the modal basis, and at frequencies of 450 Hz and 1450 Hz. The upper bound for cumulated contributions, χ_{max}, is set to 0.4, in line with the smaller bi-dimensional application. This produces a modal basis downsized from 348 modes (315 modes if considering the *a posteriori* convergence check) to 155 modes, i.e., less than 50% of its original size, for which the convergence of the solution at significant steps is presented in Figs. 10(d)–10(f). Again, while snapshots of a noticeably smoother and faster convergence are presented, monotonic convergence was observed, e.g., producing a converged solution over more than two thirds of the frequency range of interest with the first 131 sorted modes in the basis. Additionally, preliminary calculations have shown that there is a strong influence of shear waves in the porous layer in the 800–1000 Hz region, which is well captured by the mode selection procedure.

Regarding the performance of the proposed procedure, although this matter is more specifically addressed in the following section, the original problem, consisting of 1915 porous dofs, is downsized to 348 and 155 poroelastic dofs, using a truncated modal basis and a further processed modal basis, respectively. Therefore, at best, a reduction to 8% of the original size of the porous domain is achieved using the proposed method.

C. Performance estimation on a 3D test case

As a follow-up to the definition of the modal approach in Ref. 12, the same 3D application as recalled in Fig. 11 is used, with porous material 1, in order to provide performance indicators of the mode selection procedure in terms of computational time, and sparsity of the system matrix. The mesh, consisting of $8 \times 12 \times 15$ and $8 \times 12 \times 5$ eight-node hexahedric acoustic and porous elements, respectively, is considered best suited for frequencies up to 600 Hz. The modal basis including modes up to twice the highest frequency of interest is therefore composed of 800 eigenvectors. It is recalled that among those, 386 are non-orthogonal modes while the remaining 414 lead to linearly independent equations. The corresponding convergence of the reduced problem solution was presented in Ref. 12.

In a first attempt, the mode selection procedure is applied using the previously found conservative value of $\chi_{max} = 0.4$ (in the case of 2D applications) for the cumulated contributions indicator. One mode is included in the modal basis for the computation of the residual vectors. Furthermore, two residual vectors are computed at 150 Hz and 500 Hz, respectively. Applying the proposed sorting and filtering method results in a modal basis of 158 eigenvectors of which 67 are orthogonal. These imply 67 modal coordinates that can be further condensed. A comparison of the computational times, for this problem, is given in Fig. 12, where data for both the porous-treated cavity and the rigid acoustic cavity (real-valued problem) are given. The former one gives the reference computational time to be improved for the considered

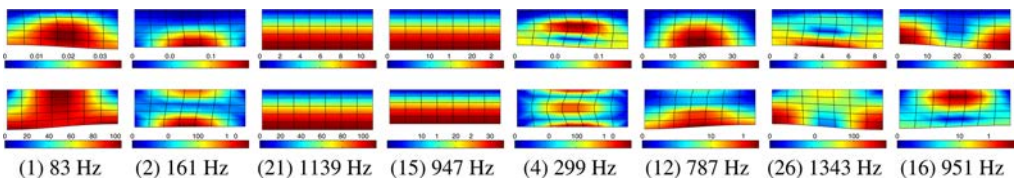

FIG. 6. (Color online) Porous 2D selected and sorted mode shapes 1, 2, 21, 15, 4, 12, 26, 16: (top) solid and (bottom) fluid phases. Deformed mesh and magnitude of displacement.

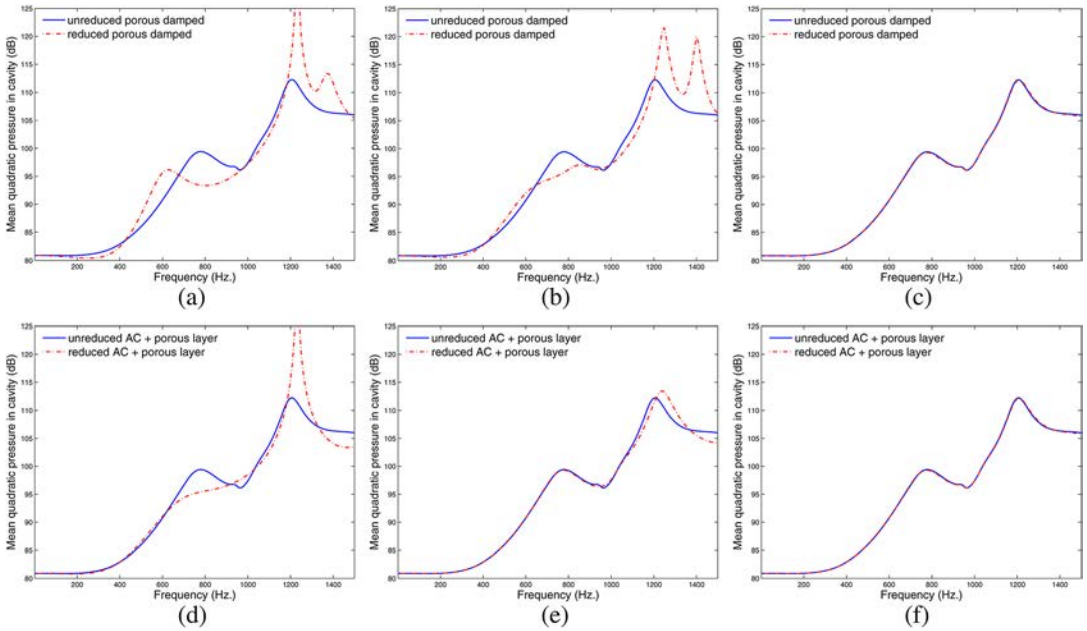

FIG. 7. (Color online) Convergence with modal superposition of non sorted modes (a)–(c) and sorted modes (d)–(f): (a) Mode 1; (b) Modes 1–15; (c) Modes 1–26; (d) Modes 1, 2, 21; (e) Modes 1, 2, 21, 15, 4; (f) Modes 1, 2, 21, 15, 4, 12, 26, 16.

problem, while the latter gives an unreachable lower bound for a reduced solution. In between, the computational times of the reduced problem using the complete set of 800 modes and the reduced set of 158 selected eigenvectors are presented. Each of these two results are completed with the corresponding version where orthogonal modes are further condensed at each frequency increment.

Several points can be noticed from the computational time improvements. First, considering the offset at the initial frequency increment for the reduced models, it appears clearly that the selection procedure proposed is comparatively costless. This is emphasized when compared to the time needed to compute the original modal basis. Second, although not showing reduction as spectacular as a 800- to 158-mode basis, the computational time enhancement is shown to be very significant, from 348 s for the original basis, to 250 s with the filtered basis, representing a 28% improvement. Of course, the fact that the 1872 acoustic dofs are kept unreduced has to be considered as a partial explanation. In addition, the reduction in the number of modes has, at some point, relatively less impact than keeping the number of attachment functions unchanged, considering the fact that they fully couple the interface dofs and the porous modal coordinates. This point is well illustrated when observing the sparsity of the unreduced and reduced problems, as shown in Fig. 13. Finally, the condensation of modal coordinates corresponding to linearly independent porous equations appears less interesting as fewer modes are included in the basis. In fact, for smaller systems to be solved at each frequency, the efficiency of the condensation becomes very dependent on the implementation of the matrix manipulations involved at each actual solution.

The sparsity and the convergence issues are addressed on a further reduced problem for which the previously found conservative value of 0.4 for $\chi_{\max}$ is not respected. Thus, for $\chi_{\max}$ set to 0.27, the precision achieved is similar up to 900 Hz while slightly inferior above—it is recalled here that the original mesh is best suited for a solution up to 600 Hz. This criterion involves 83 modes included in the basis, of which 31 imply linearly independent porous equations.

The corresponding analysis of the system matrix sparsity is presented in Figs. 13(a) and 13(c), comparing the sparsity before and after application of the mode selection procedure. It clearly shows, in this application, that the coupling involved by the 117 attachment functions at the interface acoustic dofs has a larger contribution to the solution cost than the

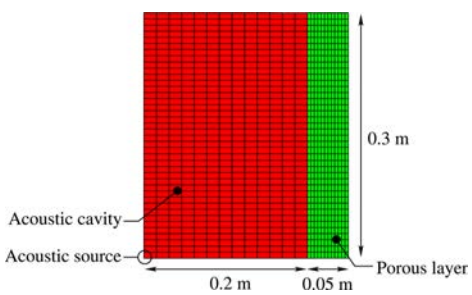

FIG. 8. (Color online) Mesh and dimensions of larger 2D application.

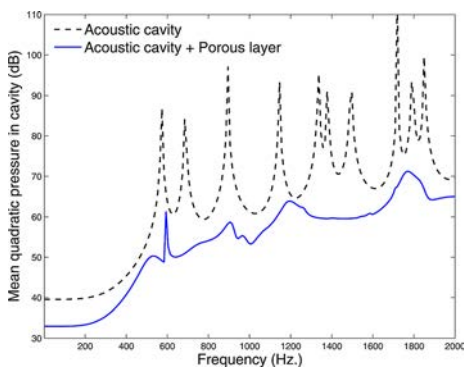

FIG. 9. (Color online) Mean quadratic pressure in the acoustic domain.

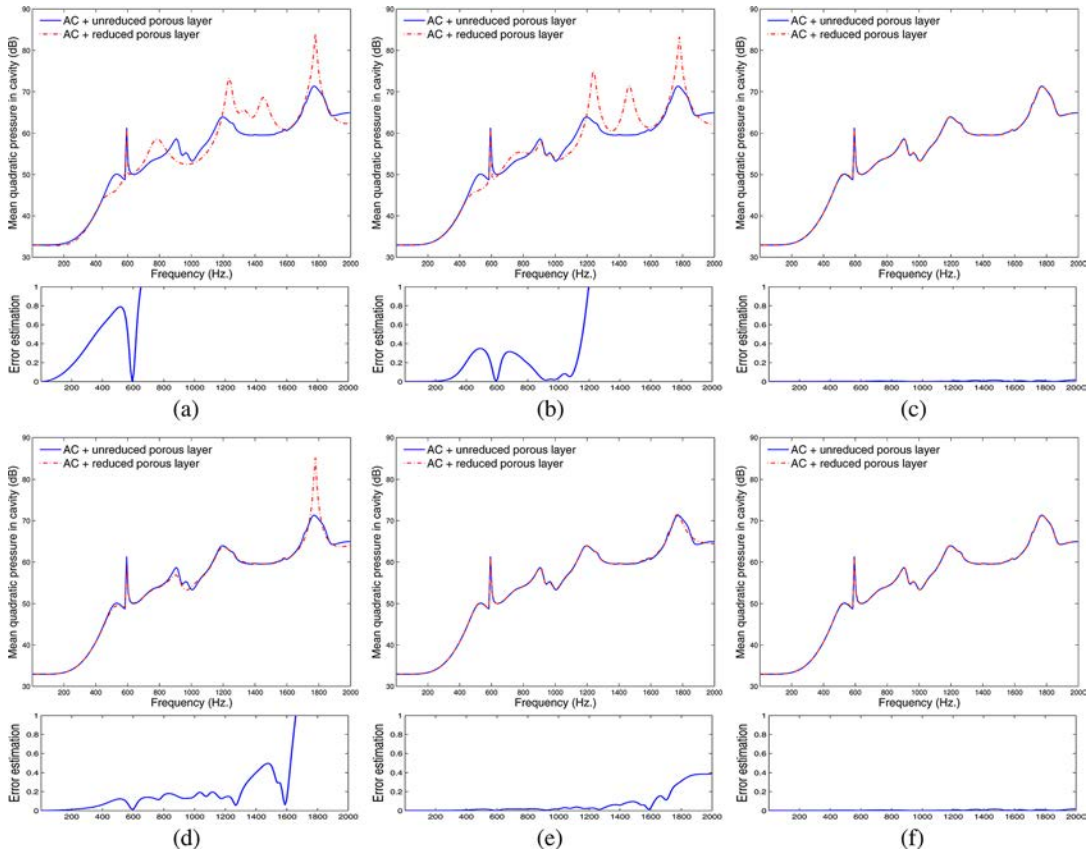

FIG. 10. (Color online) Convergence with modal superposition of non sorted modes (a)–(c) and sorted modes (d)–(f): (a) 91 modes; (b) 131 modes; (c) 315 modes; (d) 91 sorted modes; (e) 131 sorted modes; (f) 155 sorted modes.

remaining 83 porous modal dofs. This means that the use of a reduced set of attachment functions, especially in the case of large interfaces, is an important complement to the modal reduction itself. Several contributions can be found in the literature on this topic,[21,22] and applying interface condensation techniques is considered as an extension to this work.

The sparsities corresponding to the porous modal coordinates submatrices are further detailed in Figs. 13(b) and 13(d). These detailed views of the sparsity, after modal transformation of the porous equations, underline its potential in the prospect of scaling the method to larger problems. The further selection of significant modal contributions allows both for a reduction of the computational time and saves a substantial amount of memory allocated to the system matrix. For instance, in the considered application, the storage allocated to the porous subdomain after the modes selection represents a little more than 10% of the original reduction. It also illustrates the proportion of linearly independent equations kept in the process, which is very beneficial for the efficiency at larger scales.

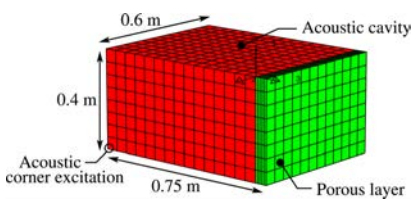

FIG. 11. (Color online) Acoustic cavity mesh and dimensions for 3D problem.

The combined analysis of the computational time and the sparsity of the reduced matrices illustrates the very promising performances of the two-step reduction method proposed. This has been further verified by the authors on a larger scale problem supporting these results. Though not included in this work for conciseness purposes, they are available in Ref. 13. Furthermore, two aspects are emphasized with the aim to further improve the reduction procedure: First, the number of attachment functions has to be kept small, as previously mentioned; then, the initial computation of the modal basis is a drawback for further improvements, especially in the scope of larger applications. Regarding this second aspect, using efficient strategies such as the Automated Multi-Level Substructuring (AMLS) method,[23] to generate approximate

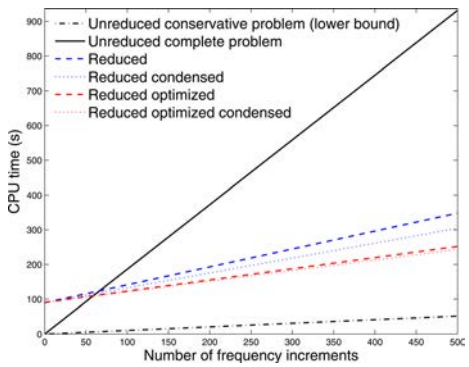

FIG. 12. (Color online) Computation time comparison for 3D problem—$\chi_{max} = 0.4$.

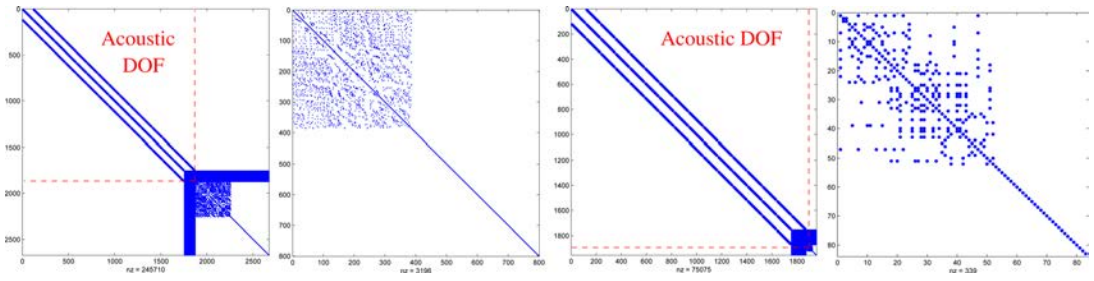

FIG. 13. (Color online) Sparsity of the system matrix and detailed sparsity corresponding to the modal DOF, before and after mode selection procedure: (a and b) 800 modes, (c and d) 83 modes.

eigenvectors, could bring substantial improvements. Another possibility is to consider a more specific way of computing the needed eigenvectors, thus reducing the initial number of modes in the basis. Load-dependent Ritz vectors generated iteratively could possibly be one way to further enhance this initial step.[24]

Finally, the convergence issue, which is however less critical than the precision and efficiency aspects, is addressed for this 3D example. Figure 14 illustrates the reduced solution obtained with (1) porous material 1 (see Table I)[20] and $\chi_{\max}$ set to 0.27, (2) porous material 2 (see Table I)[20] and $\chi_{\max}$ set to 0.3, respectively, compared to their reference solution, at significant steps of the convergence. For the latter case, using material 2, 971 modes were included in the original basis to cover twice the highest frequency of interest, thus implying three residual vectors for the mode selection procedure, calculated at 150, 500, and 750 Hz. When compared to convergence issues demonstrated in Ref. 12, the results confirm what is observed for the 2D applications: The mode selection procedure improves the mode sorting, yielding a smoother convergence with respect to the frequency. The convergence was further checked and found to be monotonic. The direct implication of these observations is that if the selection upper bound $\chi_{\max}$ was to be chosen too small (as is the case when choosing $\chi_{\max} = 0.27$ in Fig. 14), this would only have consequences for the higher frequency range of the considered problem. Truncation-wise, this places the proposed modal reduction for sound absorbing porous domains in the same context of use as traditional modal-based methods for conservative media.

V. CONCLUSION

The present work has been focused on possible remedies to the limitations raised in Ref. 12 by the authors, regarding convergence issues for the use of a modal approach to reduce

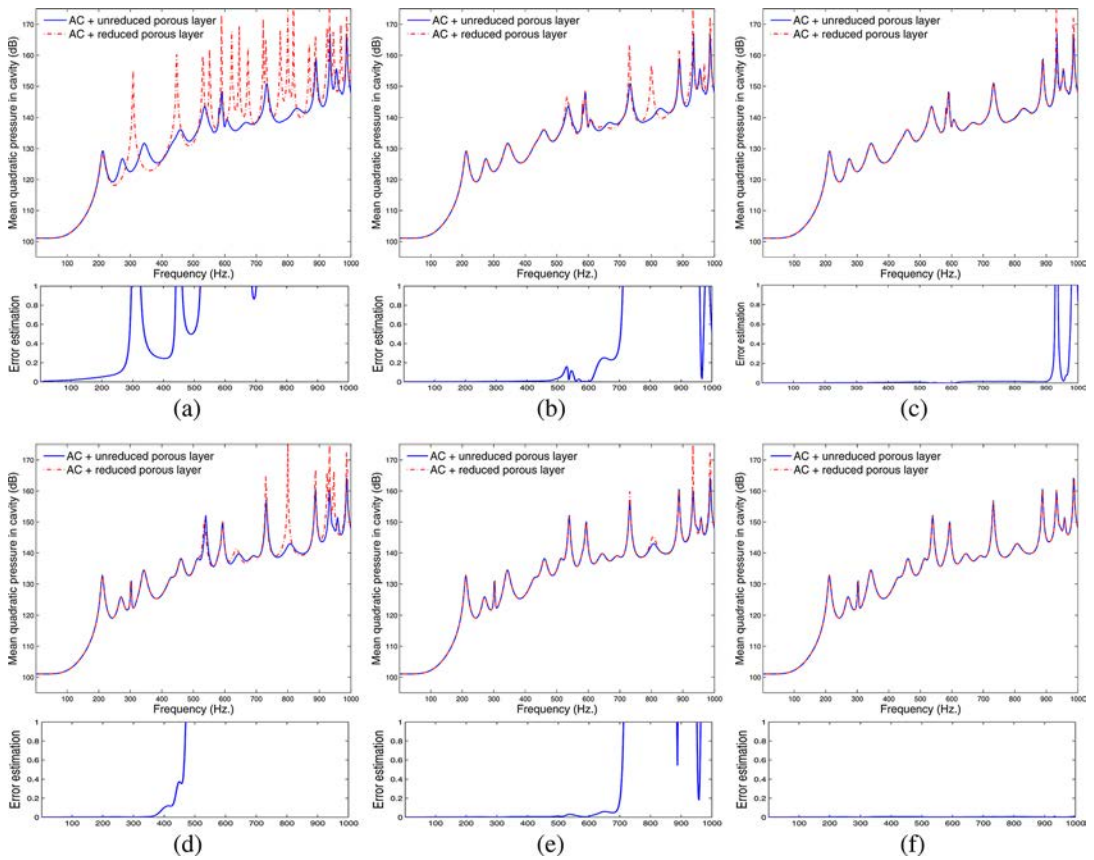

FIG. 14. (Color online) Convergence with modal superposition of selected modes for $\chi_{\max} = 0.27$, porous material 1: (a) 2 modes; (b) 58 modes; (c) 83 modes; and for $\chi_{\max} = 0.3$, material 2: (d) 45 modes; (e) 78 modes; (f) 141 modes.

poroelastic domains. For this purpose, an original sorting procedure was proposed for the modes previously selected in a truncated modal basis using a standard real-valued eigenvalue problem. This procedure is based on the modes participation to the content of a poroelastic residual force calculated from a poor approximate solution. This poor approximate solution is the outcome of a reduced model typically including the first mode in the basis. An extension to more complex problems, including a broader dynamic behavior and frequency range, was suggested and tested. It involves a procedure based on multiple residual forces calculated at different frequencies in the spectrum. The procedure was shown to properly sort the modes according to their contribution in the frequency range of the response.

Furthermore, an empirical truncation criterion was introduced, thus defining a two-step truncation procedure to establish a suitable modal basis. The first truncation, based on the standard rule of thumb stipulating that the modes whose eigenfrequencies are lower than 1.5 to 2.5 times the highest frequency of the response should be selected, ensures that the dynamic content is included in the basis. The second truncation, after applying the sorting procedure, reduces the basis to its most significant components. A validation case, including a performance analysis on a 3D academic problem, demonstrated the potential of the proposed approach: The procedure is costless when compared to the calculation of the modes, and exhibits promising performances in terms of storage and computational efficiency. A complementary larger scaled problem, to be found in Ref. 13, was tested in order to show the potential of the approach in its further extension to more complex applications. Furthermore, the modal basis thus established, being equivalent to the modal bases used in component mode synthesis techniques for conservative problems, can benefit from all the proposed modulations in the literature, among which are the following: Choice of different combinations of normal modes and interface functions, use of corrections to improve the convergence, use in a flexibility approach, etc.

There are however a few points that were addressed only as perspectives to the present work, using methods proposed in the literature. First and most importantly, the initial step, which consists in solving the eigenvalue problem, remains a drawback for extension to larger and more complex applications. For this purpose, an iterative approach could offer a possible improvement in the construction of the optimal basis. Second, porous materials are usually included into sound packages involving multilayer setups. Therefore, the reduction of the number of interface functions is of prime importance in order not to lose the benefits of the proposed approach in high surface-to-volume ratio configurations. The latter point, identified as the primary extension to be made to this contribution, concerns the applicability to more complex and industrial-like cases, which is currently under investigation after the validations proposed in this work on small 2D and 3D poro-acoustic applications.

ACKNOWLEDGMENTS

The authors gratefully acknowledge the financial and scientific support of the Marie Curie RTN and ITN projects: A Computer Aided Engineering Approach for Smart Structures Design (MC-RTN-2006-035559), and "MID-FREQUENCY – CAE Methodologies for Mid-Frequency Analysis in Vibration and Acoustics" (GA-214909), as well as the Centre for ECO^2 Vehicle Design.

[1]M. A. Biot, "Theory of propagation of elastic waves in a fluid-saturated porous solid. I. Low-frequency range," J. Acoust. Soc. Am. **28**, 168–178 (1956).
[2]M. A. Biot, "Theory of propagation of elastic waves in a fluid-saturated porous solid. II. Higher frequency range," J. Acoust. Soc. Am. **28**(2), 179–191 (1956).
[3]M. A. Biot, "Generalized theory of acoustic propagation in porous dissipative media," J. Acoust. Soc. Am. **34**(9), 1254–1264 (1962).
[4]J.-F. Allard and N. Atalla, *Propagation of Sound in Porous Media: Modelling Sound Absorbing Materials* (Wiley, New York, 2009), 372 pp.
[5]N. Atalla, M. A. Hamdi, and R. Panneton, "Enhanced weak integral formulation for the mixed (u,p) poroelastic equations," J. Acoust. Soc. Am. **109**(6), 3065–3068 (2001).
[6]Y. J. Kang and J. S. Bolton, "Finite element modeling of isotropic elastic porous materials coupled with acoustical finite elements," J. Acoust. Soc. Am. **98**, 635–643 (1995).
[7]O. Dazel, F. Sgard, and C.-H. Lamarque, "Application of generalized complex modes to the calculation of the forced response of three-dimensional poroelastic materials," J. Sound Vib. **268**(3), 555–580 (2003).
[8]P. Davidsson and G. Sandberg, "A reduction method for structure-acoustic and poroelastic-acoustic problems using interface-dependent lanczos vectors," Comput. Methods Appl. Mech. Eng. **195**(17–18), 1933–1945 (2006).
[9]C. Batifol, M. N. Ichchou, and M. A. Galland, "Hybrid modal reduction for poroelastic materials," C. R. Mécan. **336**(10), 757–765 (2008).
[10]O. Dazel, B. Brouard, N. Dauchez, and A. Geslain, "Enhanced Biot's finite element displacement formulation for porous materials and original resolution methods based on normal modes," Acta Acust. Acust. **95**(3), 527–538 (2009).
[11]O. Dazel, B. Brouard, N. Dauchez, A. Geslain, and C. H. Lamarque, "A free interface CMS technique to the resolution of coupled problem involving porous materials, application to a monodimensional problem," Acta Acust. Acust. **96**(2), 247–257 (2010).
[12]R. Rumpler, J.-F. Deü, and P. Göransson, "A modal-based reduction method for sound absorbing porous materials in poro-acoustic finite element models," J. Acoust. Soc. Am. **132**(5), 3162–3179 (2012).
[13]R. Rumpler, "Efficient finite element approach for structural-acoustic applications including 3D modelling of sound absorbing porous materials," PhD Thesis (Cnam/KTH, Paris/Stockholm, 2012), 205 pp.
[14]R. Rumpler, A. Legay, and J.-F. Deü, "Performance of a restrained-interface substructuring FE model for reduction of structural-acoustic problems with poroelastic damping," Comput. Struct. **89**(23–24), 2233–2248 (2011).
[15]G. Kergourlay, E. Balmes, and D. Clouteau, "Model reduction for efficient FEM/BEM coupling," Proc. Int. Sem. Modal Anal. **3**, 1167–1174 (2001).
[16]E. Balmes, "Modes and regular shapes. How to extend component mode synthesis theory," in *Proceedings of the XI DINAME-Ouro Preto-MG-Brazil*, 2005, 14 pp.
[17]E. Balmes, M. Corus, and S. Germes, "Model validation for heavily damped structures. application to a windshield joint," in *Proceedings of ISMA 2006*, 2006, paper 106.
[18]Q. H. Tran, M. Ouisse, and N. Bouhaddi, "A robust component mode synthesis method for stochastic damped vibroacoustics," Mech. Syst. Signal Processing **24**(1), 164–181 (2010).
[19]A. Bouazzouni, G. Lallement, and S. Cogan, "Selecting a ritz basis for the reanalysis of the frequency response functions of modified structures," J. Sound Vib. **199**(2), 309–322 (1997).
[20]N. Dauchez, S. Sahraoui, and N. Atalla, "Convergence of poroelastic finite elements based on Biot displacement formulation," J. Acoust. Soc. Am. **109**, 33–40 (2001).
[21]E. Balmes, "Use of generalized interface degrees of freedom in component mode synthesis," In *Proceedings of IMAC* (1996), pp. 204–210.
[22]J. Herrmann, M. Maess, and L. Gaul, "Substructuring including interface reduction for the efficient vibro-acoustic simulation of fluid-filled piping systems," Mech. Syst. Signal Processing **24**(1), 153–163 (2010).
[23]J. K. Bennighof and R. B. Lehoucq, "An automated multilevel substructuring method for eigenspace computation in linear elastodynamics," SIAM J. Sci. Comput. **25**(6), 2084–2106 (2004).
[24]E. L. Wilson, M.-W. Yuan, and J. M. Dickens, "Dynamic analysis by direct superposition of Ritz vectors," Earthquake Eng. Struct. Dyn. **10**(6), 813–821 (1982).